Z. Phys. A 355, 41–54 (1996)

ZEITSCHRIFT
FÜR PHYSIK A

Evidence of non-statistical structures in the elastic and inelastic scattering of ^{58}Ni+^{58}Ni and ^{58}Ni+^{62}Ni and intermediate dinuclear states

L. Vannucci[1], U. Abbondanno[2], M. Bettiolo[1], M. Bruno[3], N. Cindro[4], M. D'Agostino[3], P.M. Milazzo[3], R.A. Ricci[1,5], T. Ritz[6], W. Scheid[6], G. Vannini[2]

[1] Istituto Nazionale di Fisica Nucleare, Laboratori Nazionali di Legnaro, I-35020 Legnaro, Padova, Italy
[2] Dipartimento di Fisica dell'Università di Trieste, I-34127 Trieste, Italy and Istituto Nazionale di Fisica Nucleare, Sezione di Trieste, I-34127 Trieste, Italy
[3] Dipartimento di Fisica dell'Università di Bologna, I-40126 Bologna, Italy, and Istituto Nazionale di Fisica Nucleare, Sezione di Bologna, I-40126 Bologna, Italy
[4] Rudjer Bošković Institute, HR-41001 Zagreb, Croatia
[5] Dipartimento di Fisica dell'Università di Padova, I-35131 Padova, Italy
[6] Institut für Theoretische Physik der Justus-Liebig-Universität, D-35392 Giessen, Germany

Received: 16 October 1995 / Revised version: 20 December 1995

Communicated by C. Signorini

Abstract. Excitation functions and angular distributions of ^{58}Ni+^{58}Ni and ^{58}Ni+^{62}Ni scattering at energies just above the Coulomb barrier have been measured around θ_{cm} = 90° in energy steps ΔE_{cm} = 0.25 MeV from $E_{cm} \simeq 110$ MeV to $E_{cm} \simeq 120$ MeV for ^{58}Ni+^{58}Ni and from $E_{cm} \simeq 110$ MeV to $E_{cm} \simeq 118$ MeV for ^{58}Ni+^{62}Ni. Evidence for structure of non-statistical character has been found in the angle-summed excitation functions; this evidence is corroborated by the analysis of the angular distributions. This is the first time that non-statistical structure in elastic and inelastic scattering is reported with high confidence level for this mass and excitation energy ranges. Attempts are presented to understand the nature of this structure, including the presence of intermediate dinuclear states and virtual states in a potential well.

PACS: 25.70.Ef

1 Introduction

The resonant-like behaviour of heavy-ion collisions captured the attention of nuclear physicists since the first observation of channel-correlated structures in ^{12}C+^{12}C scattering and reactions more than a generation ago [1, 2]. Experience showed that the appearance of resonances depended strongly on the mass asymmetry parameter of the composite system, the resonant behaviour being favoured in collisions of identical nuclei [3]. The presence of resonances in the latter collisions, leading to composite systems in the mass range $A \simeq 50$ (^{24}Mg+^{24}Mg, ^{28}Si+^{28}Si), was widely reported [4–6]; however, the search for these phenomena in heavier systems has so far given negative results [7].

The early ideas of understanding the physical nature of heavy-ion resonances implied the existence of discrete states high up in the continuum, which do not mix with the surrounding high-density statistical "grass". Such discrete states should therefore be of a nature different from this "grass" and the absence of mixing would conserve their stability, hence, longevity.

A next step, taken very early in the study of heavy-ion resonances, was to associate these simple states with the so-called quasi-molecular configurations, interpreted as due to a preferential excitation of specific levels of an intermediate complex, pictured as two osculating spheres. This model successfully classified the observed resonances (in particular the ^{12}C+^{12}C resonances) in an E_x vs. $L(L+1)$ plot, with the rotational nature of resonances simply represented by the linear dependence

$$E_x = E_0 + \frac{\hbar^2}{2\mathscr{J}} \cdot L(L+1), \tag{1}$$

typical of the spectrum of a quantum rotor, with $\mathscr{J}$ the moment of inertia of two osculating nuclei.

The quasi-molecular picture, however, was by itself a crude model without predictive power. A key step forward in understanding the nature of heavy ion resonances was undertaken by the Frankfurt group [8], who introduced the concept of $molecular\ \ window$. The starting point of the concept is that if individual resonances are to be observed, their width Γ should be smaller than their spacing ΔE. The novelty introduced by the model of Ref. 8 was to assume the width Γ of a resonance to be the so-called spreading width

$$\Gamma \downarrow \sim \ iW \ = \ 2\pi \ |< \mathrm{cn} \mid V \mid \mathrm{el} >|^2 \ \rho_{cn}(E_x, L), \tag{2}$$

where W is the optical imaginary potential, $\mid el >$ and $\mid cn >$ are, respectively, the entrance (elastic) and compound nuclear states and $\rho_{cn}(E_x,L)$ is the density of levels of spin L in the composite system at the excitation energy E_x. The region of observation of resonances should then correspond to the loci of low level density ρ_{cn} in the composite system:

these loci form a window through which resonances could be seen; hence the name molecular window.

The orbiting-cluster model (OCM) of resonances, combining the molecular-window idea with the osculating-nuclei picture, was developed in the early eighties [9,10]. In spite of its simplicity, this model showed considerable predictive power for lighter systems [11] (up to ^{28}Si+^{28}Si), and was recently extended to heavier systems [12]. In this latter reference, the model served to select colliding nuclear systems leading to composite nuclei with closed neutron or proton $g_{\frac{7}{2}}$ shells (e.g. ^{28}Si+^{66}Zn leading to ^{94}Ru or ^{58}Ni+^{46}Ti leading to the neutron deficient ^{104}Sn) as favourable candidates for resonant behaviour. Later on, this calculation was extended to still heavier systems [13]. The symmetrical system ^{58}Ni+^{58}Ni turned out to be a favourable case; less so ^{58}Ni+^{62}Ni and ^{60}Ni+^{60}Ni. Specifically, the calculation predicted the occurrence of resonant states in ^{58}Ni+^{58}Ni with spin values up to about 60 $\hbar$, with rather high probability.

Interesting in this respect were the results of the measurement of ^{60}Ni+^{60}Ni elastic and inelastic scattering around the Coulomb barrier ($E_{lab} \simeq 200$ MeV) published some time ago by Erb et al. [14]. These authors reported significant differences in their data as compared with the behaviour observed in the scattering of lighter nuclei. Whereas fusion is the dominant reaction process in collisions of light nuclei in this energy range, for ^{60}Ni+^{60}Ni the quasi-elastic channels (elastic and first inelastic 2^+) dominate, being responsible for $\sim 90\%$ of the total reaction cross section.

In an earlier experiment at the Laboratori Nazionali di Legnaro (LNL, Padua, Italy) [15], two intermediate-width structures of non-statistical origin were reported at E_{cm} = 99.0 and 100.6 MeV in the elastic scattering excitation function of ^{58}Ni on ^{46}Ti measured around θ_{cm} = 90°. A statistical analysis of the angular distributions revealed periodicities of, respectively, 5.1° and 3.8° (c.m.) for the two structures. We remind that Ref. [12] predicted ^{58}Ni+^{46}Ti as a favourable case for resonance observation.

In low-energy collisions between light nuclei, the condition $\Gamma < \Delta E$ generally holds, which enables one to perform a relatively simple extraction of the spin of the resonant levels. On the contrary, in collisions between very heavy nuclei near or just above the Coulomb barrier, a complete level overlapping occurs ($\Gamma >> \Delta E$). The system displays statistical behaviour because of the incoherent contribution of various angular momenta to the process. In this case, no channel-channel correlation is expected and the angular distributions tend to be symmetrical around 90°.

The strong difference in the behaviour of the systems at the two limits makes it interesting to study the intermediate condition $\Gamma \sim \Delta E$. Level density considerations indicate that this condition of partially overlapping levels is satisfied in the mass range $A \sim 100$.

Having all this in mind, we decided to investigate the ^{58}Ni+^{58}Ni and ^{58}Ni+^{62}Ni systems. Evidence for resonances in the collisions of these relatively heavy systems would have far-reaching consequences on our understanding of the mechanism generating the resonant behaviour of heavy-ion collisions as well as on the very nature of the nucleus-nucleus interaction.

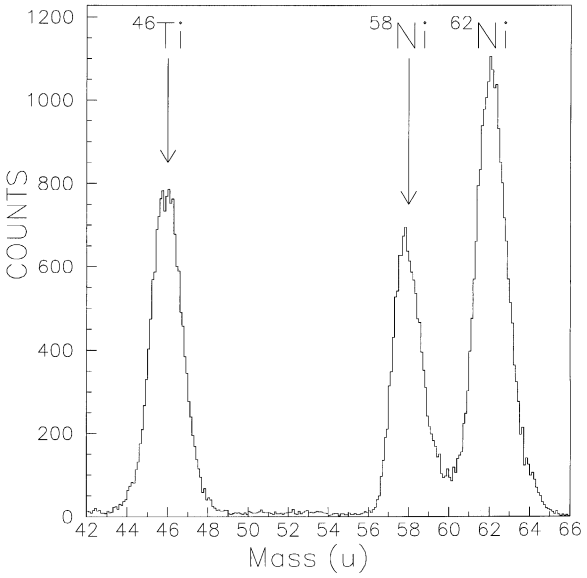

Fig. 1. The mass spectrum obtained by adding data from calibration runs performed bombarding targets of ^{46}Ti, ^{58}Ni and ^{60}Ni with a ^{58}Ni beam. The figure shows that the overall mass resolution is $\pm$1u

This article is organized as follows: The experimental set-up and the data reduction procedure are described in Sect. 2. Section 3 presents the experimental results. In Section 4 the statistical analysis of the excitation functions and of the angular distributions is given. In Sect. 5 a comparison of the experimental results with the model approaches is discussed. Finally, conclusions are given in Sect. 6.

2 Experimental

The experiment was performed at the LNL XTU Tandem accelerator. The ^{58}Ni+^{58}Ni and ^{58}Ni+^{62}Ni elastic and inelastic scattering angular distributions around θ_{cm} = 90° were measured using a ^{58}Ni beam in the laboratory energy range from 220 to 240 MeV for ^{58}Ni+^{58}Ni and from 220 to 230 MeV for ^{58}Ni+^{62}Ni. The step in the incident beam energy was 0.5 MeV in both cases. 10 μg/cm^2 ^{58}Ni and ^{62}Ni layers evaporated onto 10 μg/cm^2 carbon backing served as targets. The combined thicknesses led to an average loss in the beam energy of 130 keV over the energy range of the experiment.

The mass identification was performed using the kinematic-coincidence technique, requiring that the angles of emission and the kinetic energies of binary events should be measured in coincidence. The mass resolution was evaluated from a spectrum constructed by adding data from different runs performed with the ^{58}Ni beam incident on targets of ^{46}Ti, ^{58}Ni and ^{62}Ni. Figure 1 shows the mass resolution spectrum, Fig. 2 a composite energy spectrum corresponding to three different energies of the incident beam on ^{58}Ni.

As the experimental set-up and the data reduction procedure have been already described in detail elsewhere [16], we outline them only briefly. Two position-sensitive silicon detectors (100 μm thick, 47 mm long and 8 mm wide) were used in the experiment. The detectors for the scattered and the recoiled nuclei were placed each at angles of $\pm$45° with

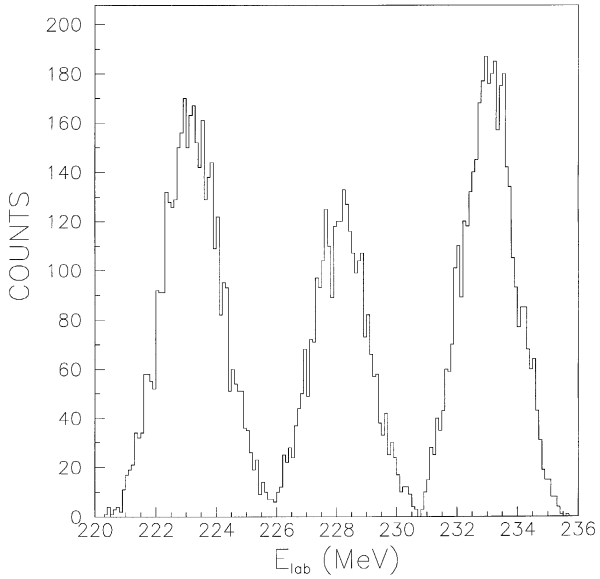

Fig. 2. Total energy spectrum of ^{58}Ni+^{58}Ni at three different beam energies. The figure shows that the overall energy resolution is about 1%

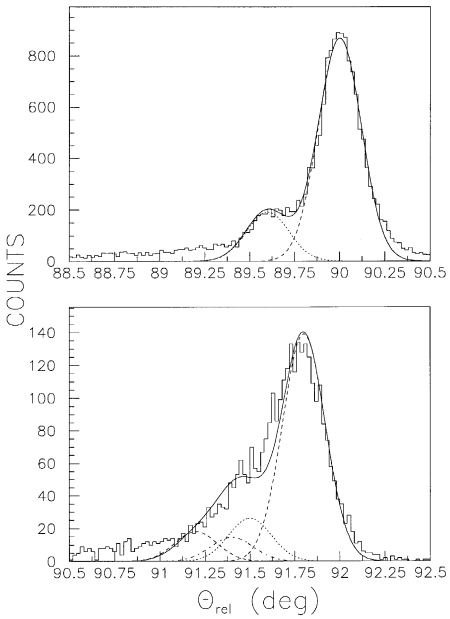

Fig. 3. The separation of the elastic and the inelastic scattering in ^{58}Ni+^{58}Ni (*top*) and ^{58}Ni+^{62}Ni (*bottom*) collisions. Broken lines represent individual channels; full lines are the sums of the single contributions

respect to the beam direction, at a distance of 155.5 mm from the centre of the target. The angular range subtended in the laboratory system for each detector was 17.2°, the subtended solid angle was 15.5 msr.

In evaluating the experimental angular resolution, the contributions of two separate effects were taken into account. The first effect is related to the intrinsic resolution ($\pm$0.5 mm) in the position information from the detectors; this effect causes an angular uncertainty $\sim 0.18°$. The second effect is due to the finite dimensions (1 mm diameter) of the beam spot; the different impact positions of the projectile on the target produce a shift of up to $\pm$0.4 mm in the detection of the scattered pair. This translates into an angular shift of $\sim 0.15°$. One should, however, stress that the first incertitude induces uncorrelated errors in the measurement of fragment emission angle whereas the second one produces shifts correlated by kinematics. Consequently, in a detection configuration symmetric with respect to the beam axis, the measurement of the laboratory relative angle (θ_{rel}) between the scattered pair is affected only by the uncorrelated errors. In our case the resolution obtained for θ_{rel} was better than $\sim 0.25°$, allowing to discriminate between the contributions of the elastic and the inelastic scatterings. Combining these data with the energy resolution (about 1%, see Fig. 2), the mass resolution turned out to be $\pm$1u.

The energy and angular calibration of the set-up was performed with particular care. This was carried out in runs where grids were placed in front of the two detectors. Precision measurements of the elastic scattering of ^{58}Ni ions from ^{46}Ti, ^{63}Cu,^{107}Ag and ^{197}Au, were performed at incident energies selected to cover the energy and angular range encountered in the ^{58}Ni+^{58}Ni and ^{58}Ni+^{62}Ni measurements. The energy and position information from the two detectors were recorded for each coincidence event; simultaneously, elastic scattering events were detected by a pair of small monitor detectors placed at $\pm$ 10° to the beam, which served to obtain both the data necessary for measuring the absolute cross sections and to monitor the beam alignment.

The energy resolution was insufficient to allow the separation of events coming from the various physical processes studied (elastic and single or mutual inelastic scattering) in terms of energy differences. Thus, we evaluated the contribution of each reaction channel to the total cross section by fitting gaussian functions to the θ_{rel} spectrum. The number of gaussians was taken to be equal to the number of channels significantly contributing to the cross section. Thus, for ^{58}Ni+^{58}Ni two gaussians were used to reproduce the θ_{rel} spectrum; the contribution of the mutual inelastic channel was too small to be taken into account. For ^{58}Ni+^{62}Ni, the data were fitted with an overlap of four gaussian functions, corresponding, respectively, to the elastic, single inelastic ^{58}Ni, single inelastic ^{62}Ni and the mutual inelastic scattering. In the fitting procedure, only the amplitudes of the gaussian functions were left as free parameters. Thus the number of events and consequently the cross sections were deduced from the amplitudes. The laboratory relative angles θ_{rel} calculated by means of the kinematics of the reaction were used as centroids of the gaussians and theirs widths are assumed equal to the FWHM of the elastic peak. Figure 3 shows the discrimination between the elastic and the inelastic scattering processes in the ^{58}Ni+^{58}Ni (top) and ^{58}Ni+^{62}Ni (bottom) scattering.

As visible from the figure, the events stemming from, respectively, the elastic and the various inelastic scatterings are not fully separated. For ^{58}Ni+^{58}Ni (Fig. 3, top) the separation is sufficient to clearly distinguish the elastic from the (first) inelastic peak and the Gaussian-fit separation is quite efficient. It is less so for the ^{58}Ni+^{62}Ni case; the uncertainties in the amplitude of the various peaks are taken into account in the systematic errors and reflects themselves in the large

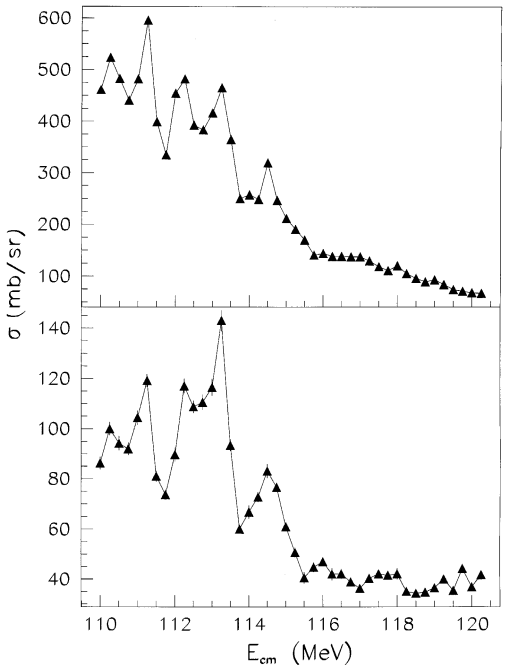

Fig. 4. Excitation functions of the angle-summed ($76° \leq \theta_{cm} \leq 104°$) elastic scattering (*top*) and inelastic (Q=-1.45 MeV) scattering (*bottom*) differential cross sections of ^{58}Ni+^{58}Ni

errors shown in the excitation functions of Fig. 8 c and d (Subsect. 3.2).

3 Results

3.1 ^{58}Ni+^{58}Ni scattering

The excitation functions of the angle-summed ($76° \leq \theta_{cm} \leq 104°$) elastic and inelastic ($Q = -1.45$ MeV first-excited level of ^{58}Ni) scattering differential cross sections of ^{58}Ni+^{58}Ni are shown in Fig.4 top and bottom, respectively. In the elastic scattering, structure appears at incident energies of 220.5, 222.5, 224.5, 226.5 and 229.0 MeV, corresponding to, respectively, 110.25, 111.25, 112.25, 113.25 and 114.5 MeV in the centre-of-mass system. All these peaks are visibly correlated with peaks observed in the inelastic scattering; we keep in mind that this correlation in various exit channels is a necessary condition for the presence of a resonance in the intermediate composite system. One should mention that the errors reported in Fig. 4 and in analogous forthcoming figures take into account both the statistical and the systematic contributions.

Figure 5 shows angular distributions of the elastically scattered ^{58}Ni on ^{58}Ni, taken at the peaks of the excitation functions in Fig. 4. Each measured angular distribution is almost perfectly fitted by squared single Legendre polynomial shapes $[P_L(\cos\theta)]^2$ with L around 60, leading to the idea of the possible presence of intermediate ($\sim$1 MeV) states. The fact that the measured angular distributions never reach zero value in their valleys is due to the finite resolution of the detectors, but could also indicate the presence of more than one partial wave contributing to the cross section. The L values were determined using the χ^2 minimization technique.

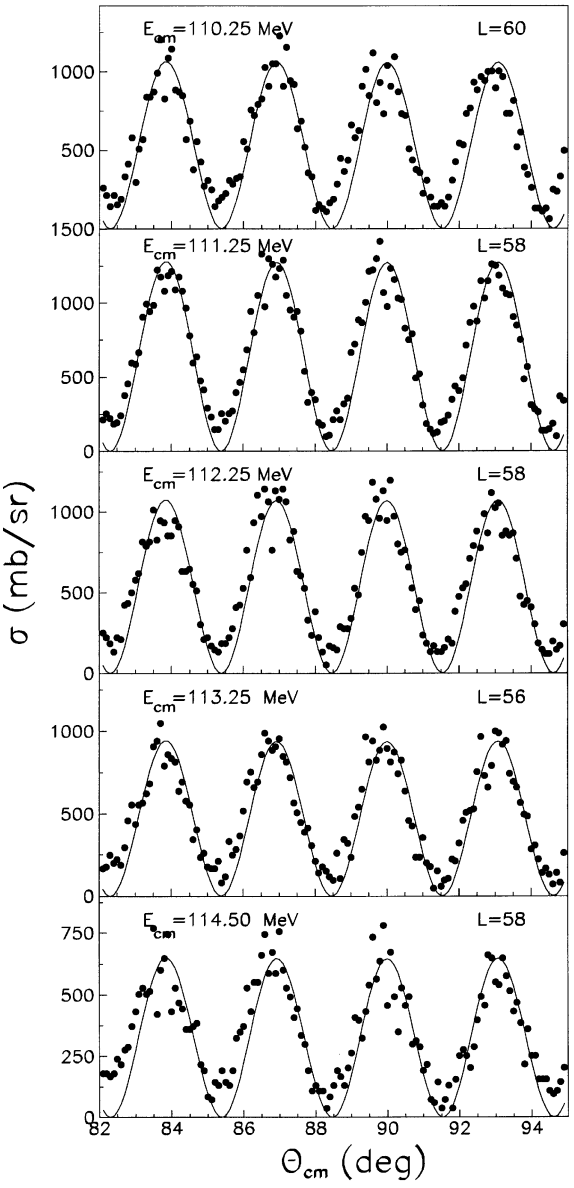

Fig. 5. ^{58}Ni+^{58}Ni elastic scattering angular distributions measured at the energies of the peaks in the elastic excitation function (Fig. 4, top). Lines are fits with a squared single Legendre polynomial of order L

It must, however, be underlined that $[P_L(\cos\theta)]^2$ shapes described well the measured elastic scattering angular distributions also at energies off the peaks in the elastic excitation function in Fig. 4, top. It is well known, furthermore, that other mechanisms produce periodic behaviour similar to that observed here. This latter point refers in particular to the fact that we deal with the scattering of identical spin-zero particles. The differential cross section for such a process, given by the general formula

$$\frac{d\sigma}{d\Omega} = \mid f(\theta) + f(\pi - \theta) \mid^2, \tag{3}$$

could exhibit interference phenomena leading to angular distributions of the same kind as those observed in this experiment. This is shown in Fig. 6, where the curves, calculated using for $f(\theta)$ the Coulomb amplitude only, reproduce the

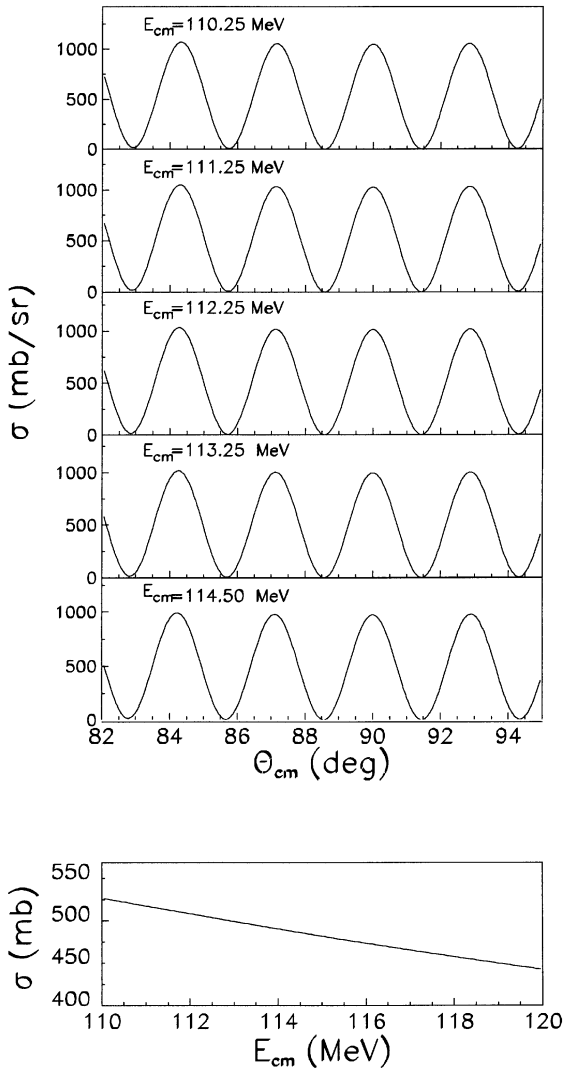

Fig. 6. Identical particles elastic scattering calculations for ^{58}Ni+^{58}Ni (Coulomb amplitude only). *Top*: angular distributions at the same energies as in Fig. 5; *bottom*: excitation function of the angle-summed differential cross sections for the above angular distributions

shape of the experimental angular distributions fairly well. The fact that the calculated angle-integrated cross section (Fig. 6, bottom), contrary to the experimental one, does not show structure in the incident energy dependence is quite understandable: the Coulomb amplitude in (3) cannot produce structure.

Figure 7 shows the inelastic ($Q = -1.45$ MeV) scattering angular distributions measured at the energies of the elastic peaks in ^{58}Ni+^{58}Ni. Direct inspection of this figure shows that the angular-periodicity is much less pronounced than in the elastic data: consequently, this data are unsuitable for a simple Legendre-polynomial fit analysis.

3.2 ^{58}Ni+^{62}Ni scattering

An obvious test of the identical-particle scattering vs. the resonance phenomenon in ^{58}Ni+^{58}Ni is the measurement of a neighbouring system such as ^{58}Ni+^{62}Ni, less favoured for

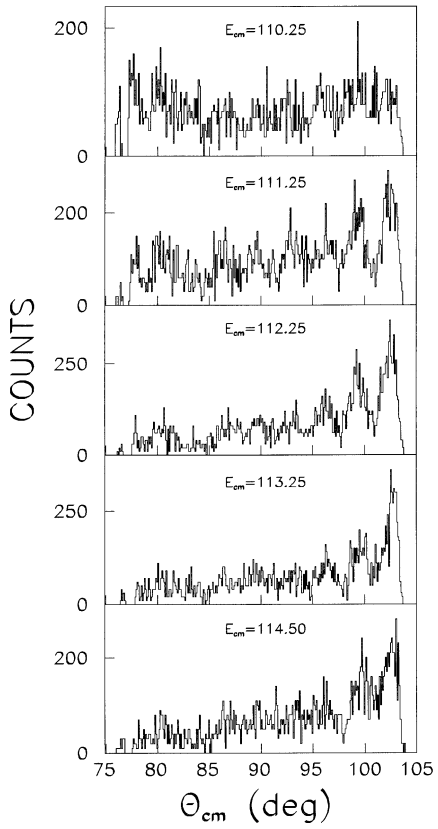

Fig. 7. ^{58}Ni+^{58}Ni inelastic scattering ($Q = -1.45$ MeV) angular distributions measured at the energies of the peaks in the elastic excitation function

resonance observation by the OCM than ^{58}Ni+^{58}Ni, but composed of two different particles. With this in mind, the elastic and inelastic scattering of ^{58}Ni on ^{62}Ni were also measured in the laboratory energy range from 220 to 230 MeV (E_{cm} = 113.7 to 118.8 MeV) in steps of 0.5 MeV.

Figure 8a–d shows the excitation functions of the various angle-summed (elastic, mutual inelastic ($Q = -(1.45 + 1.17) = -2.62$ MeV), single inelastic ^{62}Ni* ($Q = -1.17$ MeV) and ^{58}Ni* ($Q = -1.45$ MeV)) ^{58}Ni+^{62}Ni differential scattering cross sections for $72° \leq \theta_{cm} \leq 94°$. As discussed in Section 2, the large errors reported in Fig. 8 c and d are due to the uncertainty introduced in the separation of the two latter states. In the elastic and mutual inelastic scattering excitation functions (Fig. 8 a and b) where the errors are smaller, two correlated structures are clearly visible at incident ^{58}Ni energies of 224.0 and 225.5 MeV, corresponding to E_{cm} = 115.7 and 116.5 MeV, respectively.

Figure 9 shows the ^{58}Ni+^{62}Ni elastic scattering angular distributions. These distributions exhibit only weak oscillations, unsuitable for a Legendre-polynomial analysis.

4 Statistical analysis

In this Section we present the results of the analysis of the ^{58}Ni+^{58}Ni and ^{58}Ni+^{62}Ni scattering data in the frame of a statistical treatment of the excitation functions (Subsect. 4.1) and angular distributions (Subsect. 4.2). In Subsec. 4.1 we use the method adopted by D. Počanić et al. [17] and by

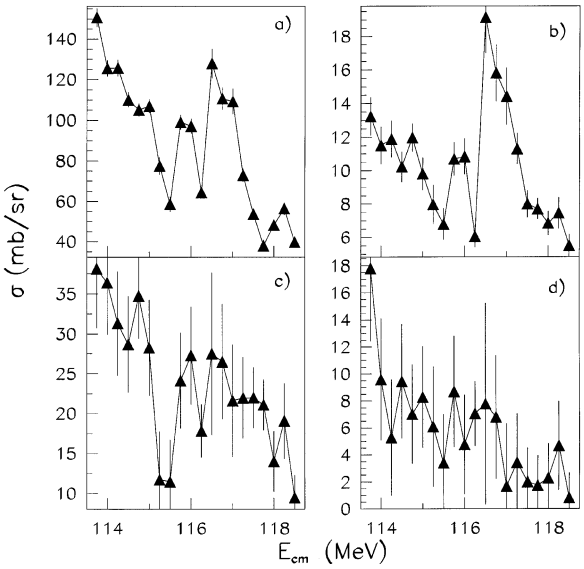

Fig. 8a–d. Excitation functions of various angle-summed ^{58}Ni+^{62}Ni scattering differential cross sections: ($72^\circ \leq \theta_{cm} \leq 94^\circ$). **a** Elastic scattering; **b** mutual inelastic scattering (Q=-(1.45+1.17)=-2.62 MeV); **c** and **d** single inelastic scattering, ^{62}Ni* (Q=-1.17 MeV) and ^{58}Ni* ($Q = -1.45$ MeV), respectively

Sarma and Singh [18], in Subsect. 4.2 the method developed by Pappalardo [19] and by Gadioli et al. [20].

4.1 Statistical analysis: excitation functions

In the first step of our analysis we attempt to separate the structures of non-statistical origin from those of statistical origin. To single out non-statistical structures in the excitation functions we use the data from two or more reaction channels and calculate:
(i) the sum of the experimental angle-summed excitation functions

$$\sigma_{tot}(E) = \sum_{m=1}^{M} (\sigma_m(E)) \,, \tag{4}$$

(ii) the summed deviation function (Ref.21)

$$D(E) \;=\; \frac{1}{M} \sum_{m=1}^{M} \left(\frac{\sigma_m(E)}{< \sigma_m(E) >} - 1 \right) \tag{5}$$

and *(iii)* the energy-dependent cross-correlation function (Ref. 21)

$$C(E) = \frac{2}{M(M-1)} \sum_{m'>m=1}^{M} \left(\frac{\sigma_{m'}(E)}{< \sigma_{m'}(E) >} - 1 \right) \times \left(\frac{\sigma_m(E)}{< \sigma_m(E) >} - 1 \right) [R_{m'}(0) R_m(0)]^{-\frac{1}{2}} \,, \tag{6}$$

where M is the total number of correlated excitation functions, $\sigma_m(E)$ the differential cross section of the m^{th} excitation function at the bombarding energy E and $< \;>$ denotes the corresponding running average over an interval ΔE_{cm}. The $R_m(0)$ and $R_{m'}(0)$ are energy-autocorrelation functions defined as

$$R_m(\epsilon) = \frac{1}{N} \sum_{n=1}^{N} \times \left(\frac{\sigma_m(E_n + \epsilon)\; \sigma_m(E_n)}{< \sigma_m(E_n + \epsilon) >< \sigma_m(E_n) >} - 1 \right) , \tag{7}$$

calculated for ϵ = 0 and called variances of the excitation functions with N measured points.

The usual criterion for the choice of ΔE_{cm} is that $\Gamma_{fine} \ll \Delta E_{cm} \ll \Gamma_{gross}$, where Γ_{fine} and Γ_{gross} are, respectively, the widths of the fine and the gross structures in the excitation functions. Following Ref. 19, we determined the value of ΔE_{cm} by the beginning of the plateau in the plot of $R_m(0)$ versus ΔE_{cm}. This plateau should be observed when ΔE_{cm} exceeds the coherence width; it corresponds to the transition point between Γ_{fine} and Γ_{gross}.

The normalized variances $R_m(0)$ for the elastic and inelastic ^{58}Ni+^{58}Ni and ^{58}Ni+^{62}Ni scatterings are plotted in Fig. 10 as functions of ΔE_{cm}. We estimated the plateaus to start at $\sim$1 MeV. Thus the value selected to average out the statistical fluctuations (fine structure) was chosen as ΔE_{cm} = 1.0 MeV, equal to four energy steps in the measurement of the excitation functions.

The basic idea underlying such an analysis is that, if structures of non-statistical nature are present, strongly correlated peaks must appear in the three functions (4), (5) and (6). Figures 11 and 12 show, top to bottom, $\sigma_{tot}(E)$ (expression (4)), $D(E)$ (expression (5)) and $C(E)$ (expression (6)) for, respectively, ^{58}Ni+^{58}Ni and ^{58}Ni+^{62}Ni. For the former system, $\sigma_{tot}(E)$ is the sum of the elastic and the inelastic ($Q = -1.45$ MeV) cross sections; for the latter, $\sigma_{tot}(E)$ is the sum of all four measured channels displayed in Fig. 8.

Figure 11 (^{58}Ni+^{58}Ni) shows correlated maxima at E_{cm} = 111.25, 112.25, 113.25 and 114.5 MeV. The analysis eliminated the peak at E_{cm} = 110.25 MeV in the $D(E)$ and $C(E)$ functions; this peak was present in the excitation functions of Fig. 4. This is due to our averaging procedure (the peak lies too close to the limit of the measuring energy interval). Fig. 12 (^{58}Ni+^{62}Ni) shows correlated maxima at E_{cm} = 115.7 and 116.5 MeV that originate from the peaks in the elastic excitation function.

To establish confidence limits of the non-statistical character of the observed structures, we have drawn the limit of 3 standard deviations on the cross-correlation functions in Figs. 11 and 12 (horizontal dashed lines, bottom). Due to the finite energy interval, the standard deviation δ_c of $C(E)$, is given by [18]

$$\delta_c = \left[\frac{2}{M(M-1)(K-1)} \right]^{\frac{1}{2}} , \tag{8}$$

where we remind that M is the number of correlated excitation functions and K the number of data points in the averaging energy interval. For the ^{58}Ni+^{58}Ni data, δ_c = 0.58; for ^{58}Ni+^{62}Ni, δ_c = 0.24. All the observed correlated peaks are outside the $3{\cdot}\delta_c$ limit, confirming with high confidence level ($\cong$ 99%) that the underlying structure is of non-statistical character. To our knowledge, this is the first time that non-statistical structures have been observed in the elastic and inelastic scattering of two medium nuclei at such high excitation energies with such a high confidence level.

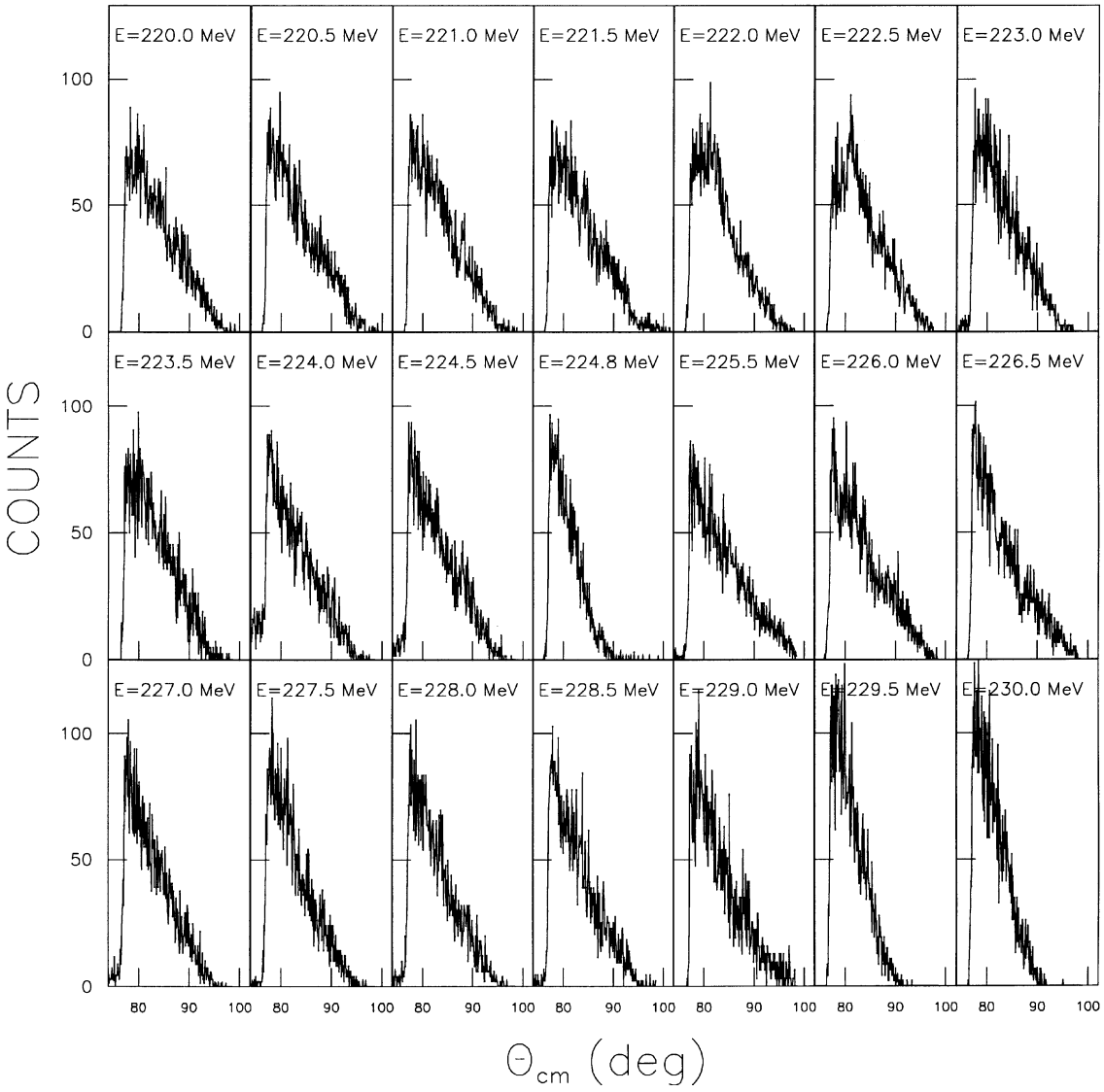

Fig. 9. Measured ^{58}Ni+^{62}Ni elastic scattering angular distributions

Table 1. Structures of non-statistical origin ($\sim$ 99% confidence level) observed in ^{58}Ni+^{58}Ni and ^{58}Ni+^{62}Ni elastic and inelastic scattering

System	E_{lab} (MeV)	E_{cm} (MeV)
^{58}Ni+^{58}Ni	222.5	111.25
	224.5	112.25
	226.5	113.25
	229.0	114.50
^{58}Ni+^{62}Ni	224.0	115.70
	225.5	116.50

The energies of the non-statistical structures are reported in Table 1. Due to the step in the measurements (ΔE_{lab} = 0.5 MeV), the energies of the correlated structures are given with an uncertainty of 0.25 MeV.

4.2 Statistical analysis: angular distributions

The aim of the analysis presented in this Subsection is to reveal periodicities in the angular distributions, and, if is possible, to relate them to the values L of the angular momenta associated with the observed structures.

The angular momentum associated to a resonant state is commonly obtained by fitting a Legendre polynomial expression to the elastic angular distribution. Various reasons, however, (the presence of identical-particle scattering, the large Coulomb scattering contribution), makes this method unsuitable for the present case. We tried to overcome this difficulty by applying to the measured angular distributions the statistical fluctuation analysis method described in Ref. 19 and 20. This method is particularly suitable to single out small intermediate-width structures as well as small-amplitude periodicities in the experimental data, minimizing the effect of uncorrelated statistical fluctuations. The original idea was to apply this method to both the ^{58}Ni+^{58}Ni and ^{58}Ni+^{62}Ni angular distributions. However, the clean periodicity present

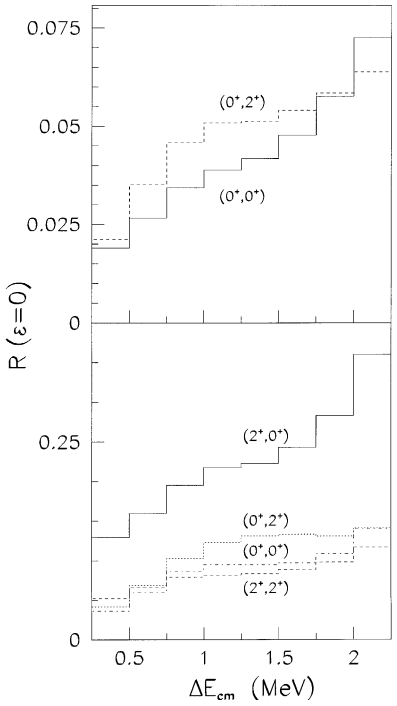

Fig. 10. Variances of the measured excitation functions $R(\epsilon{=}0)$ (Eq. (7)), plotted vs. ΔE_{cm}, for ^{58}Ni+^{58}Ni (*top*) and ^{58}Ni+^{62}Ni scattering (*bottom*)

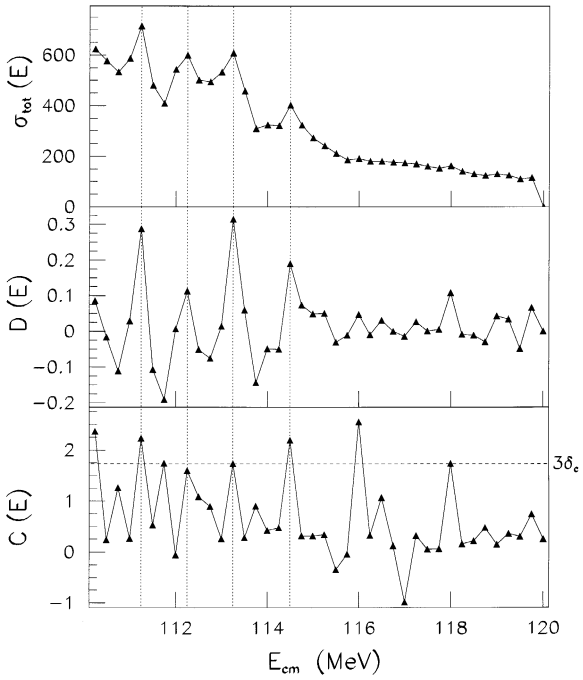

Fig. 11. Top to bottom: the angle-summed composite (elastic and all inelastics) excitation function $\sigma_{tot}(E)$ (Eq. (4)), the summed deviation function $D(E)$ (Eq. (5)) and the cross-correlation function $C(E)$ (Eq. (6)) for ^{58}Ni+^{58}Ni

in the ^{58}Ni+^{58}Ni elastic scattering angular distributions precludes the statistical analysis to yield information beyond that obtained from the Legendre-polynomial analysis; moreover, we keep in mind that the periodicity (see Subsect. 3.1.) in this latter system may stem from various causes. Thus, the statistical analysis of Refs. 19 and 20, was applied to the ^{58}Ni+^{62}Ni elastic scattering data only.

We started by calculating the variance $R(0)$ of the angular distributions $\sigma(\theta_i)$

$$R(0) \;=\; \frac{1}{I}\sum_{i=1}^{I}\left(\frac{\sigma^2(\theta_i)}{<\sigma(\theta_i)>^2}-1\right), \qquad (9)$$

where I is the number of the measured points in an angular distribution and the mean value $<\sigma(\theta_i)>$ is calculated for an average angular interval $\Delta\theta_{cm}$. Figure 13 shows $R(0)$ plotted as a function of the median angular interval $\Delta\theta_{cm}$ for the ^{58}Ni+^{62}Ni elastic data at energies corresponding, respectively, to the observed non-statistical peaks (E_{cm} = 115.7 and 116.5 MeV) as well as an energy far from the peaks (E_{cm} = 118.6 MeV). From Fig. 13 a and b we deduce that the plateau begins at roughly $\Delta\theta_{cm}$ = 2.5°; therefore this value was chosen to average out the statistical fluctuations and to calculate the autocorrelation function

$$R(\delta\theta) = \frac{1}{I}\sum_{i=1}^{I} \times\left(\frac{\sigma(\theta_i)\;\sigma(\theta_i+\delta\theta)}{<\sigma(\theta_i)><\sigma(\theta_i+\delta\theta)>}-1\right), \qquad (10)$$

in dependence on the angular interval $\delta\theta$. If the function $\sigma(\theta)$, plotted as a function of θ, has a period $\delta\theta_{per}$, the correlation function, plotted as a function of $\delta\theta$, must also display the same period $\delta\theta_{per}$ [20].

The results of this analysis applied to ^{58}Ni+^{62}Ni are shown in Fig. 14. The elastic scattering autocorrelation functions show a periodical behaviour at energies corresponding to the observed non-statistical peaks (E_{cm} = 115.7 and 116.5 MeV, Fig. 14 a and b); the periodicity is absent at energies far from the structures (E_{cm} = 118.6 MeV, Fig. 14c).

In order to extract the period of these oscillations, we calculated a $\chi^2(\theta_0)$ function which relates the values of the autocorrelation function $R(\delta\theta_j)$ at two points distant by θ_0 degrees. This $\chi^2(\theta_0)$ function is defined by

$$\chi^2(\theta_0) \;=\; \frac{1}{(J-1)}\sum_{j=1}^{J}\chi^2(\delta\theta_j,\theta_0) \;=\; \frac{1}{(J-1)}\sum_{j=1}^{J}\left(\frac{R(\delta\theta_j)\;-\;R(\delta\theta_j+\theta_0)}{\mu}\right)^2, \qquad (11)$$

where

$$\mu \;=\; \sqrt{\mu^2(\delta\theta_j)+\mu^2(\delta\theta_j+\theta_0)} \qquad (12)$$

and j is an index running over different $\delta\theta_j$. The function $\chi^2(\theta_0)$ does not depend on the angle $\delta\theta_j$ where the autocorrelation function is calculated; it depends only on the angular interval θ_0. Figure 15 shows χ^2 function calculated for the three correlation functions presented in Fig. 14 for ^{58}Ni+^{62}Ni elastic scattering, plotted as a function of θ_0. The value of χ^2 periodically reaches minima when θ_0 is equal to $\delta\theta_{per}$ or its multiples (Fig. 15 a and b). On the other hand, if no periodicity in $R(\delta\theta)$ exists, such behaviour is absent in χ^2 too (Fig. 15 c).

Table 2. Angular distribution analysis of ^{58}Ni+^{58}Ni and ^{58}Ni+^{62}Ni at the energies of the peaks in the excitation functions

System	E_{lab}(MeV)	E_{cm}(MeV)	$\delta\theta_{per}$(deg)	$L_{ded} = 180^\circ/\delta\theta_{per}$	$L_{OCM}(\hbar)$
^{58}Ni+^{58}Ni	220.5	110.25	3.0*	60±2	55
^{58}Ni+^{58}Ni	222.5	111.25	3.1*	58±2	57
^{58}Ni+^{58}Ni	224.5	112.25	3.1*	58±2	59
^{58}Ni+^{58}Ni	226.5	113.25	3.2*	56±2	60
^{58}Ni+^{58}Ni	229.0	114.5	3.1*	58±2	62
^{58}Ni+^{62}Ni	224.0	115.7	3.0$^+$	60±1	67
^{58}Ni+^{62}Ni	225.5	116.5	3.4$^+$	53±1	68

* deduced from a Legendre-polynomial analysis (Subsect. 3.1);
$^+$ obtained from the statistical analysis of angular distributions (Subsect. 4.1)

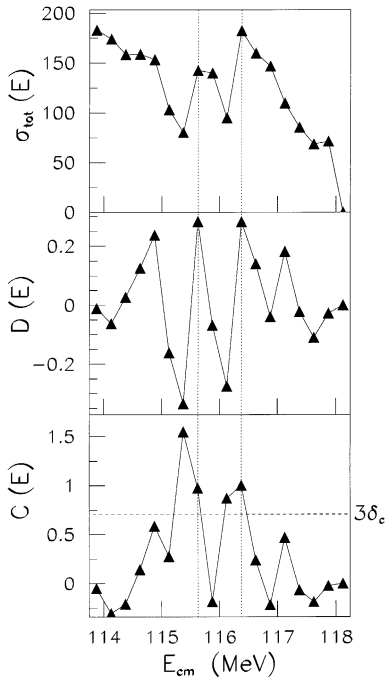

Fig. 12. Same as Fig. 11 for ^{58}Ni+^{62}Ni

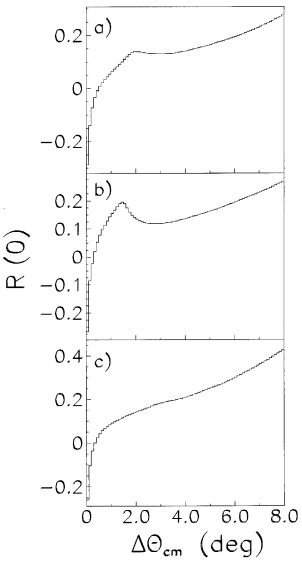

Fig. 13a–c. The angular variance $R(0)$ (Eq. (9)) plotted as a function of $\Delta\theta_{cm}$, for elastic ^{58}Ni+^{62}Ni angular distributions measured at, *top* to *bottom*, **a** E_{cm}=115.7, **b** E_{cm}=116.5 and **c** E_{cm}=118.6 MeV. The last energy is out of the range of structures seen in Fig. 11

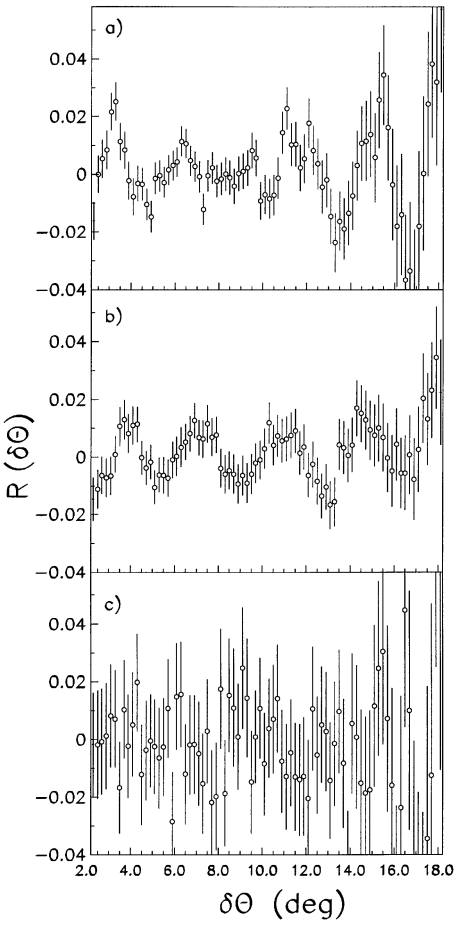

Fig. 14a–c. The angular autocorrelation functions $R(\delta\theta)$ (Eq. (10)) vs. the angular interval $\delta\theta$ calculated for the elastic scattering angular distributions of ^{58}Ni+^{62}Ni at, *top* to *bottom*, **a** E_{cm}=115.7, **b** E_{cm}=116.5 and **c** E_{cm}=118.6 MeV

The numerical value of the periodicity was determined as the average of the periods of the observed oscillations in the χ^2 functions. The uncertainty associated with this value was then assumed to be the standard deviation from this average. The extracted periodicities $\delta\theta_{per}$ are shown in Table 2 (last two rows of column 4). For completeness and comparison, values of periodicities $\delta\theta_{per}$ obtained from the Legendre-polynomial analysis of the ^{58}Ni+^{58}Ni angular distributions are reported in the same column (first five rows, denoted by asterisks).

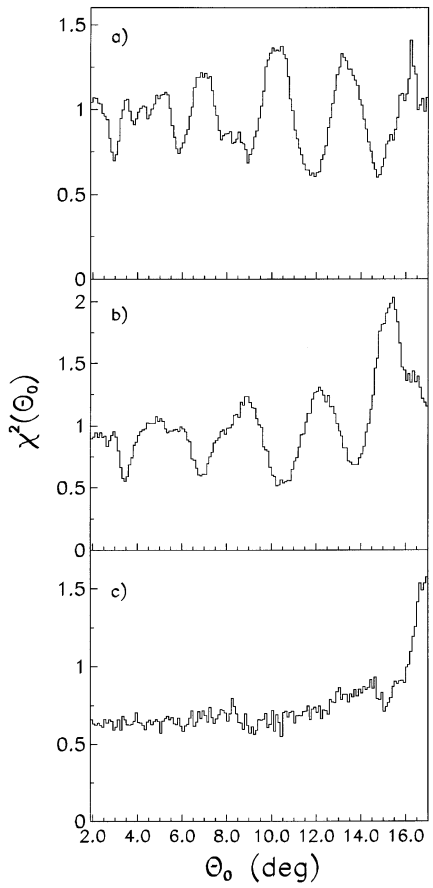

Fig. 15a–c. The values of χ^2 (Eq. (11)) plotted as a function of θ_0 for ^{58}Ni+^{62}Ni at, *top* to *bottom*, **a** E_{cm}=115.7, **b** E_{cm}=116.5 and **c** E_{cm}=118.6 MeV

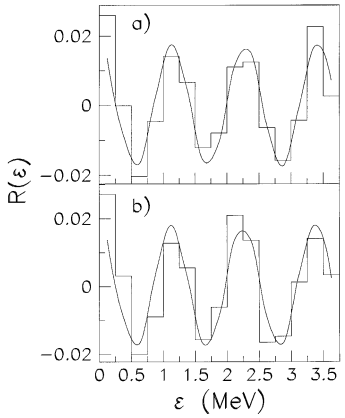

Fig. 16. *Histograms*: the energy-autocorrelation function $R(\epsilon)$ calculated for the experimental excitation functions of **a** the ^{58}Ni+^{58}Ni elastic scattering, **b** the (Q=-1.17 MeV) ^{58}Ni+^{58}Ni inelastic scattering. The sinusoidal curves are the corresponding best fits to the histograms, obtained with the reduced expression (14)

The obtained periodicities were then used to deduce a first estimate of the range of angular momenta (partial waves) effective in the scattering process. The deduced values, $L_{ded} = \frac{180^\circ}{\delta\theta_{per}}$, are also shown in Table 2. For comparison, the angular momenta L_{OCM}, predicted by the orbiting cluster model [9] (r_0=1.25 fm), are also shown in the table. We note that the values of L_{ded} for the two systems, ^{58}Ni+^{58}Ni and ^{58}Ni+^{62}Ni, are similar and that the L_{ded} and L_{OCM} values are also in resonable agreement. This consistency further corroborates the idea of underlying dinuclear rotating configurations that would be responsible for the observed structures.

5 Comparison with model approaches

In this Section we compare the experimental results with the model approach developed by Kun [22] and with a model calculation based on constructing virtual states in a potential well [23].

5.1 The intermediate dinuclear system approach

Fully equilibrated systems formed in heavy-ion collisions display random noise in the excitation functions. These (Ericson's) fluctuations show no correlation between random variables with different spin values. On the contrary, the statistical analysis of our data demonstrates the presence of channel-correlated structures in the excitation functions. This evidence is usually associated with the formation of a non-equilibrated state (doorway state) which relaxes to the compound nucleus.

In two recent papers Kun [22] proposed a model for extracting periodic, non-statistical structure from the excitation functions. In the model, the formation of an intermediate state is ascribed to the preferential excitation of dinuclear rotational states having an intrinsic wave function relatively stable to small variations of the angular velocity ω. These features involve the dependence of the energy on the angular momentum and imply a small energy dissipation in the reaction.

In such conditions, overlapping levels of rotational nature, even with different spins, originate an angular-momentum coherence of the pole form. The width of this coherence is given by the ratio γ between the total width Γ and the rotational energy spacing $\hbar\omega$ and can be estimated by means of the energy-autocorrelation function. The experimental autocorrelation functions $R(\epsilon)$ (see expression (7)) for all the measured excitation functions (elastic and inelastic) for the ^{58}Ni+^{58}Ni and the ^{58}Ni+^{62}Ni systems, are shown as histograms in Figs. 16 and 17 respectively. From the histograms a value of $\Gamma \simeq 0.6$ MeV could be extracted for the two colliding systems.

The histograms should be compared with the autocorrelation function derived in Ref. 22:

$$R(\epsilon,\theta) = Re\left[\frac{\exp(2\pi i\epsilon/\hbar\omega)}{(1-\exp(-2\pi(\Gamma-i\epsilon)/\hbar\omega))}\right] \cdot(1-\exp(-2\pi\Gamma/\hbar\omega))^2 \cdot\frac{(1-\exp(-4(\pi-\theta)\Gamma/\hbar\omega))}{\sinh(2\pi\Gamma/\hbar\omega))} \cdot(1-\exp(-2(\pi-\theta)\Gamma/\hbar\omega))^2 \quad (13)$$

which, for $\Gamma \geq \hbar\omega/2$, reduces to a simpler expression

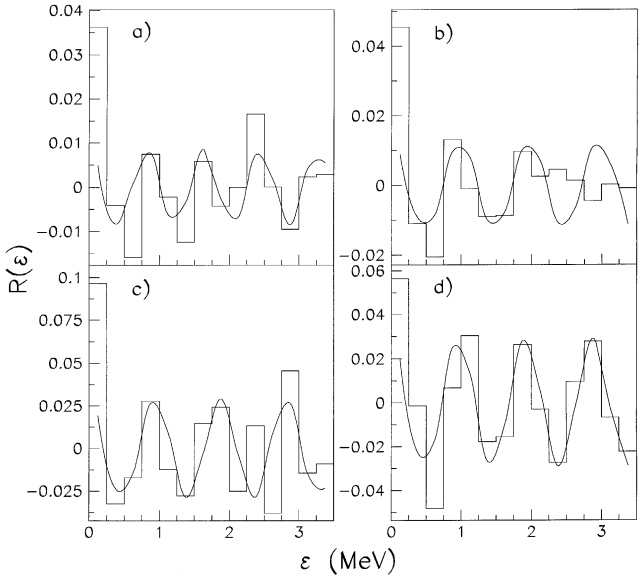

Fig. 17a–d. Histograms: the energy-autocorrelation function $R(\epsilon)$ calculated for the experimental excitation functions of **a** the ^{58}Ni+^{62}Ni elastic scattering, **b** the double (Q=-2.62 MeV) excitation, **c** the single excited level (Q=-1.45 MeV) in ^{58}Ni and **d** the single excited level (Q=-1.17 MeV) in ^{62}Ni. The sinusoidal curves are the corresponding best fits to the histograms, obtained with the reduced expression (14)

$$R(\epsilon) \simeq \exp(-2\pi\Gamma/\hbar\omega)\cdot\cos(2\pi\epsilon/\hbar\omega), \qquad (14)$$

where the magnitude of the fluctuations is considerably reduced. The associated time-power spectrum implies time-space localization, i. e. a classical picture of dinuclear rotation. Such "lighthouse effect" has been discussed previously in the literature.

The inspection of Figs. 4 and 8 reveals that, in our case, $\Gamma \geq \hbar\omega/2$, so expression (14) could be used to fit the experimental energy-autocorrelation functions in Figs. 16 and 17. In the fit procedure two parameters in expression (14) were let free: the angular velocity ω and the total width Γ. The calculated behaviour of $R(\epsilon)$ is displayed as solid curves in Figs. 16 and 17, together with the histograms calculated using the experimental data (expression (7)). The results of the fit are reported in columns 2 and 3 of Table 3.

Table 3 also reports the life-times τ of the studied systems, calculated as $\hbar/\Gamma$ and, tentatively, the average orbital momenta $L_{stat} = \mathscr{J}_{rel}\omega/\hbar$, associated with several elastic and inelastic states. In the calculation, $\mathscr{J}_{rel}$ was assumed by Ref. 22 to be the moment of inertia of the relative (orbital) motion of the two colliding nuclei. The internuclear distance used in calculating $\mathscr{J}_{rel}$ was the same as that used in calculating $\mathscr{J}$ in the OCM model [9], with r_0=1.25 fm in both cases.

It is gratifying to find that the values of the angular momenta (active partial waves) deduced from this analysis are compatible with those obtained by the statistical analysis of the angular momentum distributions (compare Table 2 with the results of Table 3).

The satisfactory agreement between the experimental and the calculated energy autocorrelation functions indicates that, within the framework of the model of Ref. 22, the studied scattering processes proceed through the selective excitation of rotational dinuclear states and that more than a single wave contributes. Moreover the comparable magnitude of $\hbar\omega$ and Γ points out to only partial overlapping of the excited states. Consequently, the non-statistical fluctuations present in the excitation functions should be due to the angular momentum correlation.

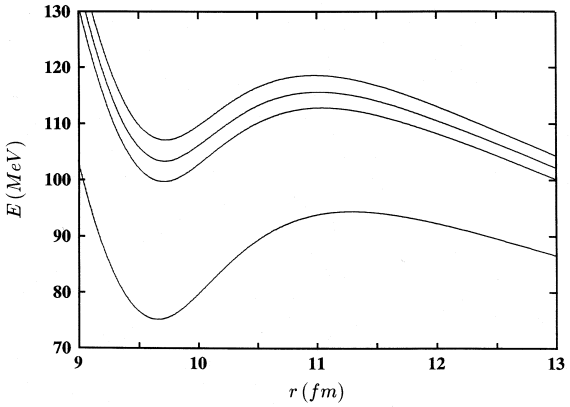

Fig. 18. Calculated ^{58}Ni+^{58}Ni interaction potentials for values of the angular momentum L=64$\hbar$, 60$\hbar$ and 56$\hbar$. The lowest curve is for L=0

From Table 3 it appears that the decay of both systems, ^{58}Ni+^{58}Ni and ^{58}Ni+^{62}Ni is rather rapid (order of 10^{-21} s), testifying of the short life-time of the rotational dinuclear system. Even so, however, the high values of the angular momenta lead to a mean rotational angle, not negligible also for life-times of the order of 10^{-21} s. In fact, from the product $\tau\omega$, one infers that the intermediate dinuclear system decays after about a quarter of a complete rotation ($\simeq$ 1.5 radian). This indication is coherent with the decreasing trend of the angular distributions such as measured for the ^{58}Ni+^{62}Ni system. The behaviour is typical of peripheral collisions where a narrow window of waves contributes to the reaction. Ref. 23 shows that the partial overlapping of levels having a common rotational character produces angular distributions with focusing effects typical of the deep inelastic dissipative phenomena, instead of the $[P_L(\cos\theta)]^2$ shapes expected in the zero-spin channel.

The analysis in the framework of Ref. 22, speaks in favours the conclusion that the gross oscillations of the angular distributions in the ^{58}Ni+^{58}Ni elastic scattering are due to identical-particle interference rather than to a resonant single partial wave.

Finally, we stress that the macroscopic rotations in the formalism of Ref. 22 are a quantum phenomenon that generates non-statistical fluctuations in the excitation functions because of the spin-spin interference. In this sense, the resulting intermediate configurations, considered as "macroscopic quasi-molecular states" are of a nature fundamentally different from that of the intermediate heavy-ion resonances with fixed spin and parity.

5.2 Virtual states in a potential well

We shall now discuss another approach based on the search for pockets in the interaction potential of the two colliding nuclei. Such pockets would generate quasi-bound states and

Table 3. Best-fit parameters and related quantities from the autocorrelation analysis of ^{58}Ni+^{58}Ni and ^{58}Ni+^{62}Ni, using Eq. (14)

System	Best-fit values Γ(MeV)	Best-fit values $\hbar\omega$(MeV)	Calculated $\mathscr{J}_{rel} = \mu R^2$($10^{-41}$ MeV s^2)	$L_{stat} = \mathscr{J}_{rel}\omega$ ($\hbar$)	$\tau = \hbar/\Gamma$ (10^{-22} s)
^{58}Ni+^{58}Ni	0.73	1.14	2.80	73	9.0
^{58}Ni*+^{58}Ni	0.72	1.12	2.80	72	9.1
^{58}Ni+^{62}Ni	0.59	0.82	2.97	56	11.2
^{58}Ni*+^{62}Ni*	0.68	0.98	2.97	67	9.7
^{58}Ni+^{62}Ni*	0.54	0.96	2.97	66	12.2
^{58}Ni*+^{62}Ni	0.53	0.94	2.97	64	12.4

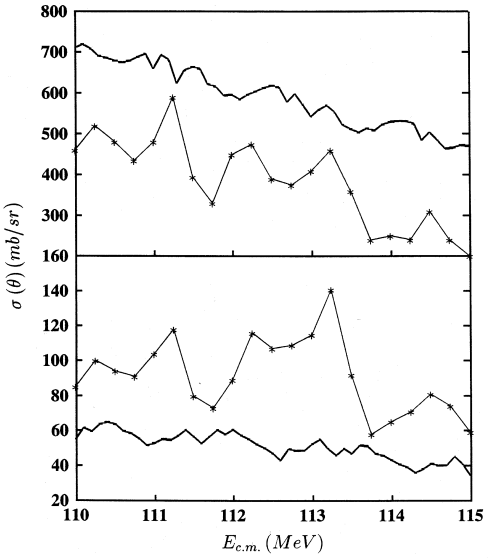

Fig. 19. Angle-summed elastic and inelastic ^{58}Ni+^{58}Ni cross sections calculated with the potential of Fig. 18. *Upper part*: elastic cross section, *lower part*: inelastic cross section for the 2^+ excitation of ^{58}Ni. The cross sections are summed between θ_{cm}=76° and 104° and compared with the experimental data represented by *asterisks* connected with a *thin line*

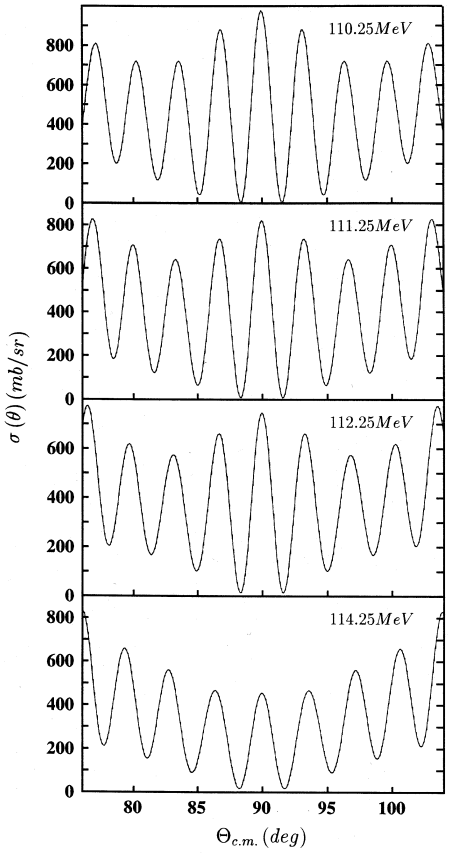

Fig. 20. Calculated elastic angular distributions of ^{58}Ni+^{58}Ni at E_{cm}=110.25, 111.25, 112.25 and 114.25 MeV (energies of the peaks in the elastic excitation function)

virtual resonances responsible for the structure observed in the excitation functions of the angle-summed data. Virtual states near the Coulomb barrier were predicted by Könnecke et al. [24] to generate structure around E_{cm}=110 MeV in the ^{60}Ni+^{60}Ni elastic scattering.

In the present work we calculate the folding potential for ^{58}Ni+^{58}Ni (Fig. 18) for values of the angular momentum from L=56$\hbar$ to 64$\hbar$. The barriers of the calculated potentials were about 114 MeV high. The potential for L=0, also shown in Fig. 18, was calculated by a double-folded Yukava-integral in the sudden approximation [25]. The parameters of the two Yukava forces were μ_1=0.60 fm, V_1=-8300 MeV fm and μ_2=0.40 fm, V_2=21500 MeV fm. The density of the Ni nuclei was assumed to be homogeneous; the nuclear radius was assumed equal to 4.92 fm. Using the real potentials of Fig. 18 we carried out coupled channel calculations of the ^{58}Ni+^{58}Ni scattering cross sections. In these calculations, the imaginary part of the optical potential is set to zero. Partial waves up to L=80 were summed.

The resulting excitation function of the elastic and inelastic scattering do show structures, but less pronounced than in the experimental data (see Fig. 19; in the figures the asterisks connected by the thin lines represent the experimental data). On the other hand, elastic angular distributions of ^{58}Ni+^{58}Ni calculated using the same above potential reveal periodical behaviour (Fig. 20) similar both in shape and average periodicity to those experimentally observed.

6 Conclusions

In this paper we present data on the ^{58}Ni+^{58}Ni and ^{58}Ni+^{62}Ni scattering, taken just above the Coulomb barrier. The data consist of angular distributions measured around θ_{cm}=90° in narrow energy steps ($\Delta E_{cm} \sim 0.25$ MeV) and of excitation functions obtained by summing the measured differential cross sections over the entire angular range covered. These data were used in a search for possible intermedi-

ate configurations in the composite systems, the presence of which was suggested by phenomenological models [12,13].

Essentially all the measured Ni+Ni scattering channels (elastic and inelastic) show structure in the respective excitation functions. Thus, our first step was to analyse the excitation functions of the different Ni+Ni scattering channels, using statistical methods that permit to single out structure of non-statistical character. Combining informations from the total excitation function $\sigma_{tot}(E)$, the deviation function $D(E)$ and the cross-correlation function $C(E)$ [21], we identified a total of 7 structures in the two colliding systems. For 6 of them, we could say with at least a 3 standard-deviation level of confidence ($\sim$ 99% confidence level) that they were not of statistical origin. To our knowledge, this is the first time that an extensive analysis has brought up convincing evidence for non-statistical structures in this mass and excitation energy range. The energies of these structures are reported in Table 1.

The second step in our analysis was to examine the structures by comparing the angular distributions at on- and off-peak energies. Angular distributions of elastically scattered ^{58}Ni+^{58}Ni showed almost perfect squared single Legendre-polynomial shapes; however, such shapes are also expected from quantum identical-particle scattering and cannot be taken as signatures of intermediate resonant states. Moreover, these perfect shapes are present in the elastic angular distribution both at the on- and the off-peak energies. On the other hand, the angular distributions of the ^{58}Ni+^{62}Ni elastic scattering show periodicity solely at the energies of the structures; this periodicity, however, could be identified only through a statistical analysis of the angular distributions. The results of this analysis are shown in Table 2. They corroborate the findings of the statistical analysis of the excitation functions, indicating that the resonant phenomenon, if present, is associated with a narrow window of high angular momenta rather than with a single spin.

Next we turned to exploring the underlying physical nature of the structures. Thus, as a third step we compared the results of our statistical analysis with two theoretical approaches. The first approach, developed by Kun [22] for extracting periodic non-statistical structure from a statistical background, explains the correlations in terms of the presence of rotating intermediate dinuclear states. A comparison was made between the calculated and the experimental energy-correlation functions for various measured excitation functions. In this comparison, the quantities Γ (the width of the structures) and $\hbar\omega$ (the energy of the intrinsic excitation of intermediate structures) were left as free parameters of a fit procedure. Good fits were obtained for most of the experimental correlation functions. The obtained best-fit values of Γ and $\hbar\omega$ for the various systems are essentially those that could be guessed from the experimental excitation functions themselves. Typical values for, e.g., the ^{58}Ni+^{58}Ni system are $\Gamma \sim 0.7$ MeV and $\hbar\omega \sim 1$MeV. These values are listed in Table 3, together with other physical quantities that could be derived from them.

The second approach treats the problem of intermediate structure starting from pockets in the interaction potential of the two colliding nuclei [24]. Such pockets generate quasi-bound states - similar in their nature to shape isomers - that produce structure in the excitation function and periodicity in the angular distributions. The calculated excitation functions show structure, albeit somewhat less pronounced than the experimental data. On the other hand, the elastic angular distribution of ^{58}Ni+^{58}Ni calculated with this model, reveals periodical behaviour very similar in shape and periodicity to the experimental one.

A last point to stress is the consistency of the values of L obtained from various sources in the analysis. These values are most reasonably interpreted as the average of a narrow range of coherent partial waves active in the process [22]. The fact, therefore, that they are mutually consistent and, moreover, consistent with angular momenta obtained from the Orbiting Cluster Model of Ref. 9, is quite gratifying. To wit: for ^{58}Ni+^{58}Ni, the average value of L_{ded}, deduced from the angular distribution periodicity, is $\sim$ 58, the model value obtained from the statistical excitation function analysis [22] is $L_{stat} \sim 72$, and the model value predicted by the OCM is also $\sim$ 58. The corresponding numbers for ^{58}Ni+^{62}Ni are $\sim$ 57 for L_{ded}, $\sim$ 63 for L_{stat} and $\sim$ 67 for L_{OCM}.

To summarize, we point out

– the high level of confidence (99%) for the non-statistical nature of the structure observed in ^{58}Ni+^{58}Ni and ^{58}Ni+^{62}Ni scattering excitation functions,
– the good agreement of the fits based on Eq. (14) with the correlation functions constructed from the ^{58}Ni+^{58}Ni and ^{58}Ni+^{62}Ni data,
– the agreement between the experimental cross sections and those calculated with the pockets-in-the-potential approach (^{58}Ni+^{58}Ni only),
– the consistency of values of L deduced from the analysis of the angular distributions, those obtained from the energy-autocorrelation function analysis (Eq. (14)) and those calculated with the OCM.

These features strongly support the idea that the observed structures (Table 1) are due to the presence of an intermediate phenomenon in the composite systems. This phenomenon would stem from the coherent effects of a narrow range of partial waves active in the process. Its nature is compatible with the formation of a dinuclear quasi-molecular-type configuration.

We would like to thank the skilful collaboration of the LNL Tandem crew. The technical assistance of Mr. Galliano Busacchi is also gratefully acknowledged. Thanks are also due to Dr. Z. Basrak for calculating the identical-particle scattering angular distributions and their excitation function and to Mr. K. Šparavec for supplying us with his OCM calculations for the Ni isotopes. We are very much indebted to Dr. S. Yu. Kun for several illuminating discussions. One of us (N. C.) acknowledges the financial assistance of the INFN and the hospitality of the LNL during his visit to this laboratory.

References

1. Bromley, D.A., Kuehner, J.A., Almqvist E.: Phys. Rev. Lett. **4**, 365 (1960); Almqvist, E., Bromley, D.A., Kuehner, J.A.: Phys. Rev. Lett. **4**, 515 (1960)
2. For a recent review of the subject see, e.g., Abbondanno, U., Cindro, N.: Int. Jour. Mod. Phys. **E2**, 1 (1993)
3. Betts, R.R.: Nucl. Phys. **A447**, 257c (1985)
4. Zurmühle, R.W., Kutt, P., Betts, R.R., Saini, S., Haas, F., Hansen, O.: Phys. Lett. **129B**, 384 (1983)

5. Saini, S., Betts, R.R., Zurmühle, R.W., Kutt, P.H., Dichter, B. K.: Phys. Lett. **185B**, 316 (1987)
6. Betts, R.R., DiCenzo, S.B., Petersen, J.F.: Phys. Lett. **100B**, 117 (1981)
7. Kutt, P.H., Pate, S.F., Wuosmaa, A.H., Zurmühle, R.W., Hansen, O., Betts, R.R., Saini, S.: Phys. Lett. **155B**, 27 (1985)
8. Scheid, W., Greiner, W., Lemmer, R.: Phys. Rev. Lett. **25**, 176 (1970)
9. Cindro, N., Počanić, D.: J. Phys. G **6**, 359 (1980)
10. Počanić, D., Cindro, N.: Nucl. Phys. **A433**, 531 (1985)
11. Abbondanno, U.: Phys. Rev. **C43**, 1484 (1991)
12. Cindro, N., Božin, M.: Ann. Phys. (N.Y.) **192**, 307 (1989)
13. Šparavec, K.: Rudjer Bošković Institute, POB 1016, Zagreb, Croatia, private communication
14. Erb, K.A., Ford, J.L.C. Jr., Novotny, R., Shapira, D.: in Resonances In Heavy Ion Reactions, ed. by K.A. Eberhard, Lecture Notes in Physics **156**, 204 (1982)
15. Abbondanno, U., Demanins, F., Vannini, G., Boccaccio, P., Vannucci, L., Ricci, R.A., Bruno, M., d'Agostino, M., Milazzo, P.M., Cindro, N.: Int. Jour. Mod. Phys. **E3**, 919 (1994)
16. Abbondanno, U., Demanins, F., Vannini, G., Vannucci, L., Boccaccio, P., Donà, R., Ricci, R.A., Božin, M., Cindro, N.: J. Phys. **G16**, 1517 (1990)
17. Počanić, D., Čaplar, R., Vourvopoulos, G., Aslanoglou, X.: Nucl. Phys. **A444**, 303 (1985)
18. Sarma, A., Singh, R.: Z. Phys. **A337**, 23 (1990)
19. Pappalardo, G.: Phys. Lett. **13**, 320 (1964)
20. Gadioli, E., Iori, I., Mangialaio, M., Pappalardo, G.: N. Cim. **38**, 1105 (1965)
21. Dennis, L.C., Thornton, S.T., Cordell, K.R.: Phys. Rev. C **19**, 777 (1979)
22. Kun, S. Yu.: Phys. Lett. **B257**, 247 (1991), Europhys. Lett. **26**, 505 (1994)
23. F. Rizzo, G. Cardella, A. De Rosa, A. Di Pietro, A. D'Onofrio, E. Fioretto, G. Inglima, A. Musumarra, M. Papa, G. Pappalardo, M. Romano, M. Romoli, F. Terrasi, M. Sandoli and G.S. Wang
Z. Phys. **A349** (1994) 169
24. Könnecke, R., Greiner, W., Scheid, W.: in Nuclear Molecular Phenomena, ed. by Cindro, N., North Holland Publ. Co., Amsterdam 1978, pg. 109
25. Broglia , R.A. and Winther, A.: in Heavy Ion Reactions vol. I, Benjamin/Cummings Publ., Amsterdam 1981